Subgrid Scale Physics in 1-Month Forecasts. Part II: Systematic Error and Blocking Forecasts

K. MIYAKODA AND J. SIRUTIS

Geophysical Fluid Dynamics Laboratory/NOAA, Princeton University, Princeton, New Jersey

(Manuscript received 21 August 1989, in final form 25 November 1989)

ABSTRACT

The capability of blocking prediction is investigated with respect to four models of different subgrid scale parameterization packages, which were described in Part I. In order to assess the capability, blocking indices are defined, and threat and bias scores are set up for the predicted blocking index against the observation. Applying this evaluation scheme to the dataset of one-month forecasts for eight January cases, we conduct a study on the performance of blocking simulation.

First, it is immediately disclosed that the systematic biases in this forecast set are overwhelmingly large, so that the blocking index has to be adjusted to this bias. One of the major issues, suggested by Tibaldi and Molteni, is whether the systematic bias is generated by the failure of blocking forecasts. Overall, this study supports this assertion, despite the different definitions of blocking. The study also reveals that the A-model is inferior to the other three models, such as the E-model, with regard to blocking forecasts. The reason for this is that the E-model, for example, which includes turbulence closure parameterization, appears to provide an adequate conversion of low-frequency eddy potential to kinetic energy, and thereby produces a more reasonable amount of standing eddies related to the persistent ridges. It is also pointed out that the blocking activity in the winter Northern Hemisphere is manifested by a distinct subpolar peak in the meridional distribution of standing eddy kinetic energy. The E-model tends to generate a well-defined peak of this energy distribution. All models are deficient in expanding the zonal mean westerlies to higher latitudes, particularly the A-model. In this connection, a hypothesis is postulated on a precondition for blocking: the upstream westerlies prior to the onset have to be displaced relatively at lower latitude. In the successful cases of blocking forecasts, the upstream westerlies at 40°–60°N are relatively weaker than those in the unsuccessful cases.

1. Introduction

Medium-range forecasts in operational centers have improved appreciably in the last 10 years (for example, see Arpe 1988), yet the useful skill of forecasts is still limited to on average 6 or 7 days. Concerning one-month forecasts, experiments have been performed by several groups around the world, for example, the United States, western Europe (ECMWF, England, and France), and Japan. The current status is, however, that the skill of 10 day mean forecasts remains marginal at the end of one month (for example, Hollingsworth et al. 1987). Miyakoda et al. (1986) commented that the current general circulation model (GCM) includes a great deal of systematic bias and the results of forecasts cannot be improved without removing a substantial part of this bias.

In the meantime, a view has emerged that, in order to create a breakthrough to this impasse both for the medium-range and one-month range, the simulation of blocking processes has to be improved. Tibaldi and

Corresponding author address: Dr. Joseph Sirutis, Geophysical Fluid Dynamics Laboratory, P.O. Box 308, Princeton University, Princeton, NJ 08542.

Molteni (1988), after extensive study of the performance of the ECMWF forecasts on the blocking ridge, concluded that the systematic bias is mostly produced during blocked situations, and, in particular, the bias reflects the incapability of the model to enter the blocked state.

For the improvement of blocking forecasts, at least four prediction elements are relevant: the refinement of subgrid scale (SGS) physics, the increase of the model's spatial resolution (e.g., Tibaldi and Ji 1983), the application of more appropriate external forcings, and the improvement of initial condition. The external forcings could be any of the orographic effect, the sea surface temperature anomalies, the soil moisture anomalies, and the snowmelt anomalies, while the issue of initial data is to improve the ability to define adequately the initial conditions relevant to the precursory elements such as the cold surge or the "bomb" (see Sanders and Gyakum 1980).

In Part I of the present paper (Sirutis and Miyakoda 1990), four packages of SGS physics parameterization, i.e., the A, the E, the F and the FM, have been applied to 1-month forecasts for eight January cases, and the forecasting performances have been investigated. On the other hand, the simulation of an outstanding blocking case was discussed by Miyakoda et al. (1983),

and a hypothesis was proposed: a GCM with "advanced" physics is more capable than a model with "inferior" physics in simulating blockings. Figure 1 displays an example showing that the E-physics outperforms the A-physics. The figure is the 10 day mean wind fields for the case of January 1977, which are represented by the streamlines on the 500 hPa level between the equator and 60°N latitude. The simulations are for the 20–30 day means of 1-month forecasts. In the reality and the successful E-model prediction, one observes high–low couplets, which are referred to as a "Modon" by McWilliams (1980), whereas, in the unsuccessful A-model prediction, the flow tends to be zonal.

The importance of SGS physics is reexamined here based on eight January cases. Thus Part II is a study of the capability of blocking forecasts from the standpoint of SGS physics parameterization using a dataset of 1-month forecasts. The eight cases consist of 1 January 1977, 1978, 1979, 1980, 1981, 1982 and 1983, and 16 January 1979 [referred to as 1979(16)] as the initial time; each case includes three slightly different initial conditions.

2. Simulation of blockings

a. Blocking indices

The conventional method for the determination of a blocking signature is to identify a positive geopotential height anomaly (ridge), and to examine the duration of this anomaly (Rex 1950; Hartmann and Ghan 1980; Treidl et al. 1981; Dole and Gordon 1983; Shukla and Mo 1983; Knox and Hay 1985).

In this paper, the 500 hPa geopotential height, z, on a 4° by 4° regular latitude–longitude grid is taken, and the height anomalies are calculated by

$$\delta Z = z - z_n, \qquad (2.1)$$

where the subscript n denotes the climatological norm. Using this anomaly a determination is made as to whether blocking is taking place or not based on two different methods.

1) METHOD IA

First, check whether the anomaly exceeds a specified value at any of two particular central latitude points, ϕ_N and ϕ_S, a central longitude point, λ_0, and their surrounding gridpoints, i.e.,

$$\delta Z(\lambda, \phi) \geqslant \delta Z_{crit}, \qquad (2.2)$$

where λ and ϕ are the longitude and the latitude, and

$$\phi_N = 60°N + \Delta,$$

$$\phi_S = 45°N + \Delta,$$

$$\lambda = \lambda_0 + \Delta, \qquad (2.3)$$

and any of $\Delta = -4°, 0°$ or $4°$. Second, examine whether this outstanding ridge continues to stay at the same location or $\pm 4°$ neighborhood longer than a specified number of days. If these two conditions are satisfied, the ridge is defined as "blocked"; otherwise it is regarded as a transient ridge.

In practice, we adopted

$$\delta z_{crit} = 120 \text{ m, and}$$

$$\text{Duration} = 8 \text{ days.} \qquad (2.4)$$

2) METHOD IIA

As another method, we use here the similar approach as Tibaldi and Molteni (1989). In this study, the 10 day mean geopotential height, $\bar{z}^{10}$, at 500 hPa, as opposed to the daily value, is used. The height, $\bar{z}^{10}$, on a 4° by 4° regular latitude–longitude grid is taken, and the blocking index of Lejenäs and Økland (1983) is calculated. The geopotential gradient, GHGS, is defined by

$$\text{GHGS} = (z(\phi_N) - z(\phi_S))/(\phi_N - \phi_S), \qquad (2.5)$$

where

$$\phi_N = 60°N + \Delta$$

$$\phi_S = 40°N + \Delta,$$

and $\Delta = -4°, 0°$ or $4°$. A given longitude is then defined as "blocked" if the following condition is satisfied for at least one value of Δ:

$$\text{GHGS} > 0. \qquad (2.6)$$

Let us denote this method as Method IIa.

The solid lines in Figs. 2a and 2b show the longitudinal distributions for the frequency of observed blocks during a month of the eight January cases, based on Methods Ia and IIa, respectively. The figure indicates that (i) in Method Ia, the North Atlantic is the primary zone for blocking and the Aleutian area is secondary, while in Method IIa, this order is reversed; (ii) the frequency curves obtained by Methods Ia and IIa do not agree with each other; and (iii) the frequencies of blockings in this paper are rather high (the maximum is about 50%), compared with other authors, for example, Treidl et al. (1981), in which the maximum frequency is about 20%, the reason being the value of δZ_{crit} in Eq. (2.2) (in their case $\delta Z_{crit} \sim 200$ m).

We next apply Methods Ia and IIa to the GCM simulations. The dashed lines in Figs. 2a and 2b show the blocking frequency for the E-model. This figure clearly shows that the models are deficient in generating or maintaining blocks at the observed frequencies; however, inspection immediately reveals that the selection standard for blocking in Methods Ia and IIa are too severe because the models' geopotential height includes an appreciable magnitude of systematic errors. This was already pointed out by Mansfield (1986) and
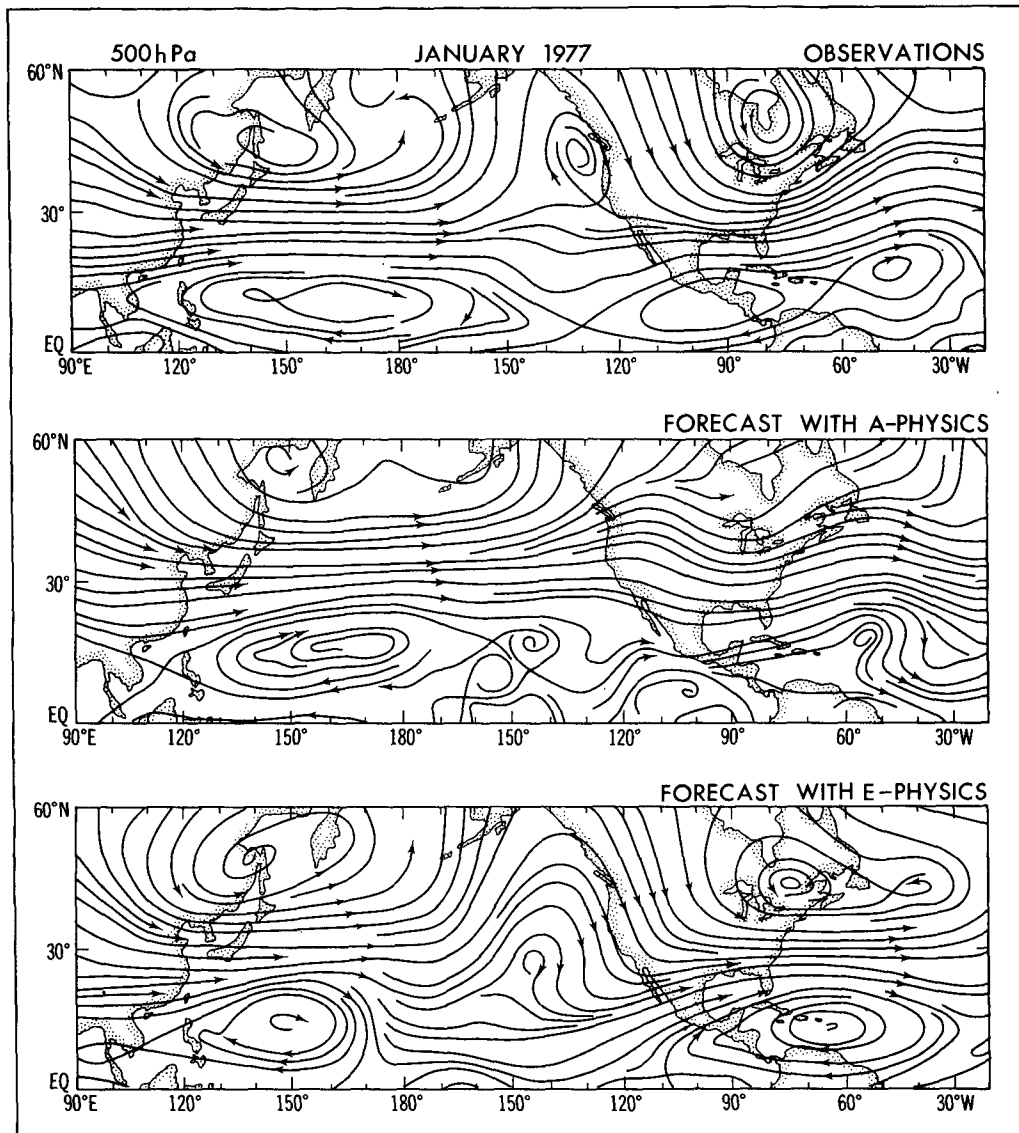
FIG. 1. The wind fields are shown by 10-day mean streamlines for the third ten days (20–30 days) of 1-month predictions. The NMC observation (top), the A-model (middle), and the E-model (bottom). (After Miyakoda et al. 1983.)

Blackmon et al. (1986); the model blocks are generally in the right longitudinal positions, but the simulated heights are too low, and the patterns are not maintained long enough.

3) METHODS IB AND IIB

Thus, taking the model's systematic bias into account, the predicted geopotential heights are first adjusted for "climate drift":

$$z_{adj.} = z - (\Delta z)_{drift}, \qquad (2.7)$$

where $(\Delta z)_{drift}$ is the systematic error given by Eq. (3.3) in Part I. $(\Delta z)_{drift}$, which is average over the four models of different parameterizations (A, E, F and FM), is a function of geographical location and forecasting time. It is natural that the climate drift is relatively small in the early part of the forecast, and increases appreciably later. In practice, we took the 5-day average of the systematic error for a 1-month forecast range. This value, $z_{adj.}$, is used for z in (2.1). We denote this procedure as Method Ib or Method IIb, when the scheme is applied to Method I or II, respectively.

The dash-dotted lines in Figs. 2a and 2b are the percentage frequency of blocking in the model based on Methods Ib and IIb, respectively. These frequencies agree better with the observation than those obtained by Methods Ia and IIa.
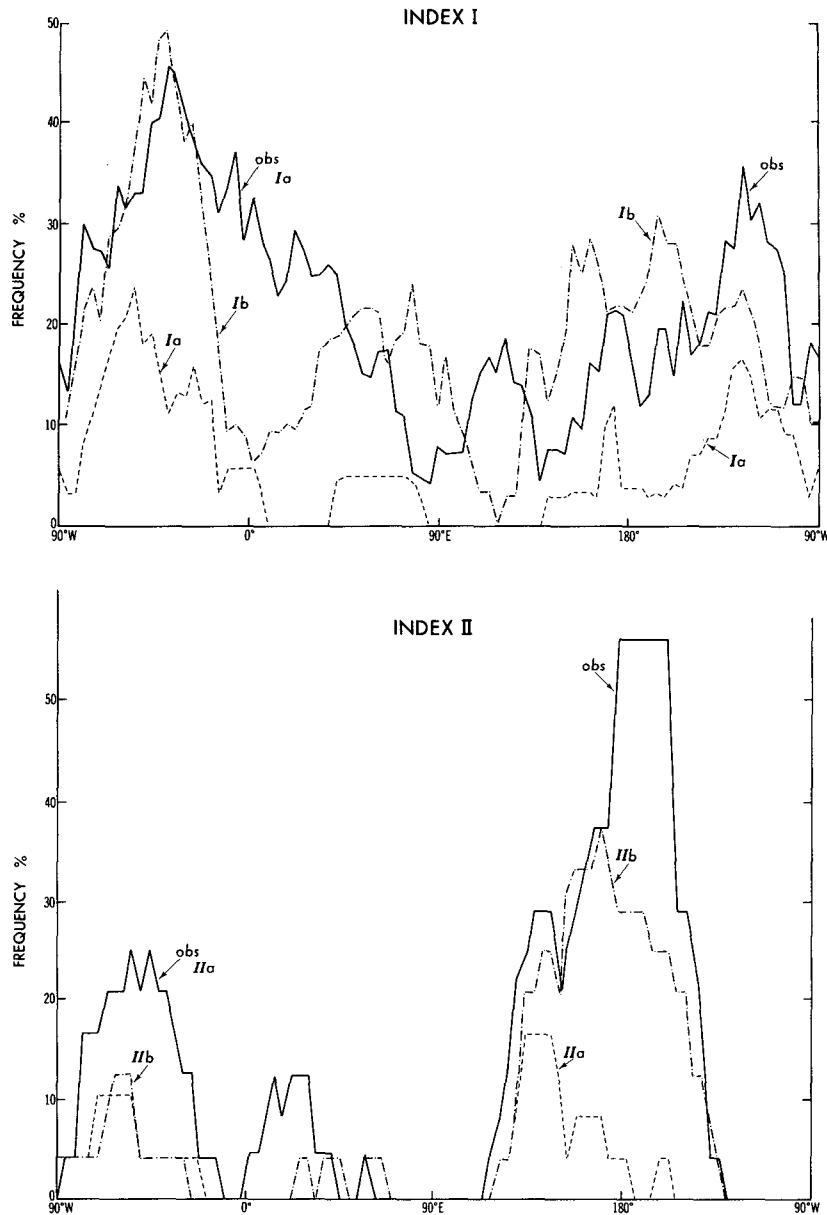
FIG. 2. (a) Percentage frequencies of blocking, identified by Method I for eight January cases. The abscissa is longitude. The observation based on Method Ia is shown by the solid line. The model results are determined by Method Ia (– – –) and Ib (– · – · –). (b) The same as panel (a), but the blockings are identified by Method II.

b. Skill scores

Figure 3 illustrates how the blocking signature is determined by Method Ia, taking as an example the case of January 1977. The upper panel of Fig. 3 delineates the area in the longitude–time chart representing the 500 hPa height anomalies exceeding the criterion, 120 m, in Eq. (2.2). Based on this chart, the blocking episode is determined in the lower panel by checking whether the shaded regions in the upper panel persist for more than 8 days.

Let A denote the blocking area thus determined in units of percentage, relative to the total diagram space, i.e., 360° longitude × 30 days. The average percentage area, A, for the 8 cases in this study is 18%. The areas, A, for the individual cases are listed in Table 1. As is seen, the largest appearance of blocking is found in the case of 1981, while the least amount is in the case of 1978.

Figure 4 displays four comparisons of the forecasted blocking signature by the E-model (right) with obser-

NMC ANALYSIS JANUARY 1977
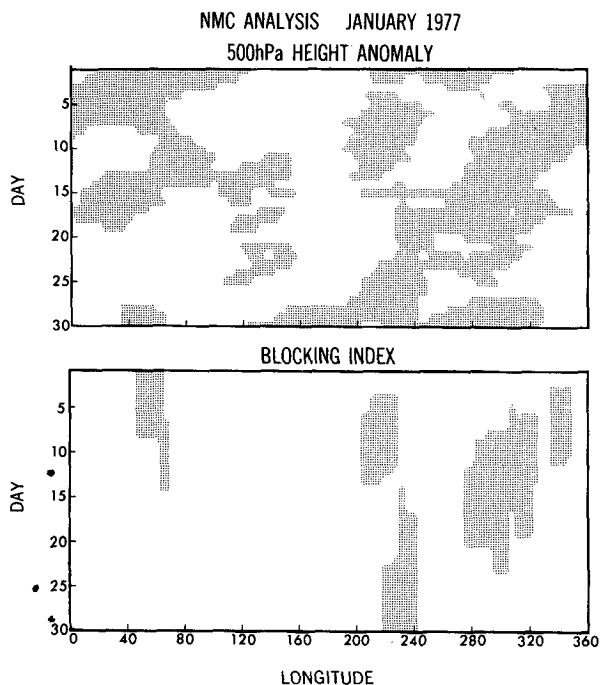500hPa HEIGHT ANOMALY

BLOCKING INDEX

LONGITUDE

FIG. 3. The procedure of Method I for determination of blocking. The abscissa is longitude going eastward from the prime meridian, and the ordinate is forecast time. The 500 hPa height anomalies above 120 m in the longitude–time space (upper panel) are shaded, and the blocking ridges, which are determined if the height anomalies above 120 m persists for more than 8 days (lower panel), are shaded.

vations (left). Method Ia is employed for the observation, while Method Ib is used for the forecasts.

In order to have a measure of the performance of blocking simulation, "threat" scores of the blocking area between the forecast and the verification are calculated by the formula

$$\text{Threat} = \frac{A_C}{A_F + A_0 - A_C}, \qquad (2.8)$$

where A_F and A_0 are the areas of blocking in the longitude–time diagram for the forecast and the verification (NMC analysis), respectively, and A_C is the area of blocking commonly occupied by both the forecast and the verification. The scores for the E-models are plotted at the lower left corner in Fig. 4. In this example, the threat scores indicate that the prediction of blocking was fairly good for the 1977 and 1979(16) cases, while the prediction was poor for the 1978 case. It is understood from Fig. 4, however, that the poor score in the 1978 case is due to rare occurrences of blocking.

Another measure is the "bias," which is defined by

$$\text{Bias} = A_F / A_0. \qquad (2.9)$$

Tables 2 and 3 are the lists of threat scores for the models' results based on the identification of blocking signatures in various selection methods. The results of bias score are listed in Table 4. In these tables, the

results of the four models, A, E, F and FM, are shown. As described in Part I, the SGS physics is more sophisticated in the order from the A to the FM model, and it was hoped that the performance would be improved stepwise in this order. Reality, however, does not follow expectation. Inspecting these tables, one notes the following: (i) The highest threat scores are found mostly in the E and sometimes in the FM, and the lowest is always in the A; (ii) overall, the FM does increase the capability of the simulation of blocks, compared with the F, indicating that the "envelope mountain" in the FM enhances the blocking activity; (iii) the selection procedure of IIa/IIa at the left of Table 4 indicates that only 22% of observed blocking signatures are captured by the forecasts, while the selection procedures of IIb/IIa at the right gives as much as 85% (111% in the FM), implying that the systematic biases seriously affect the blocking identification; and (iv) the E-model performs much better than the A-model from the standpoint of bias score.

Let us now turn to Fig. 5, in which the time evolutions of blocking are represented by indices, i.e., the percentage area, A, in Method Ia for the observation and Method Ib for the models' results. The abscissa is the forecasting time for 30 days. The indices, A, are averaged over the entire globe for every day and also over eight January cases. If the sample number is sufficiently large, the evolution of the index should be constant in time, because the occurrence of observed blocks is randomly distributed within the month, i.e., there is no preferred time climatologically for the emergence of blocks. The exception is the edge-effect at both ends of the 1-month period. This edge-effect originates from the definition of the blocking in Methods Ia and Ib, i.e., the more-than-8-day duration of anomaly high. At any rate, this figure gives another indication that the E-model is more capable of generating and maintaining the blockings than the A-model, especially after about day 12.

3. Systematic errors

a. Stratification by the blocking index

In order to examine the assertion of Tibaldi and Molteni (1989) that the systematic error is mostly associated with the failure to forecast the onset of blocking, we calculate the forecast errors in our dataset by stratifying the errors in terms of the degree of failure/ success in blocking forecasts. The errors we are con-

TABLE 1. The blocking activity shown by the blocking ridge area, A, in percent.

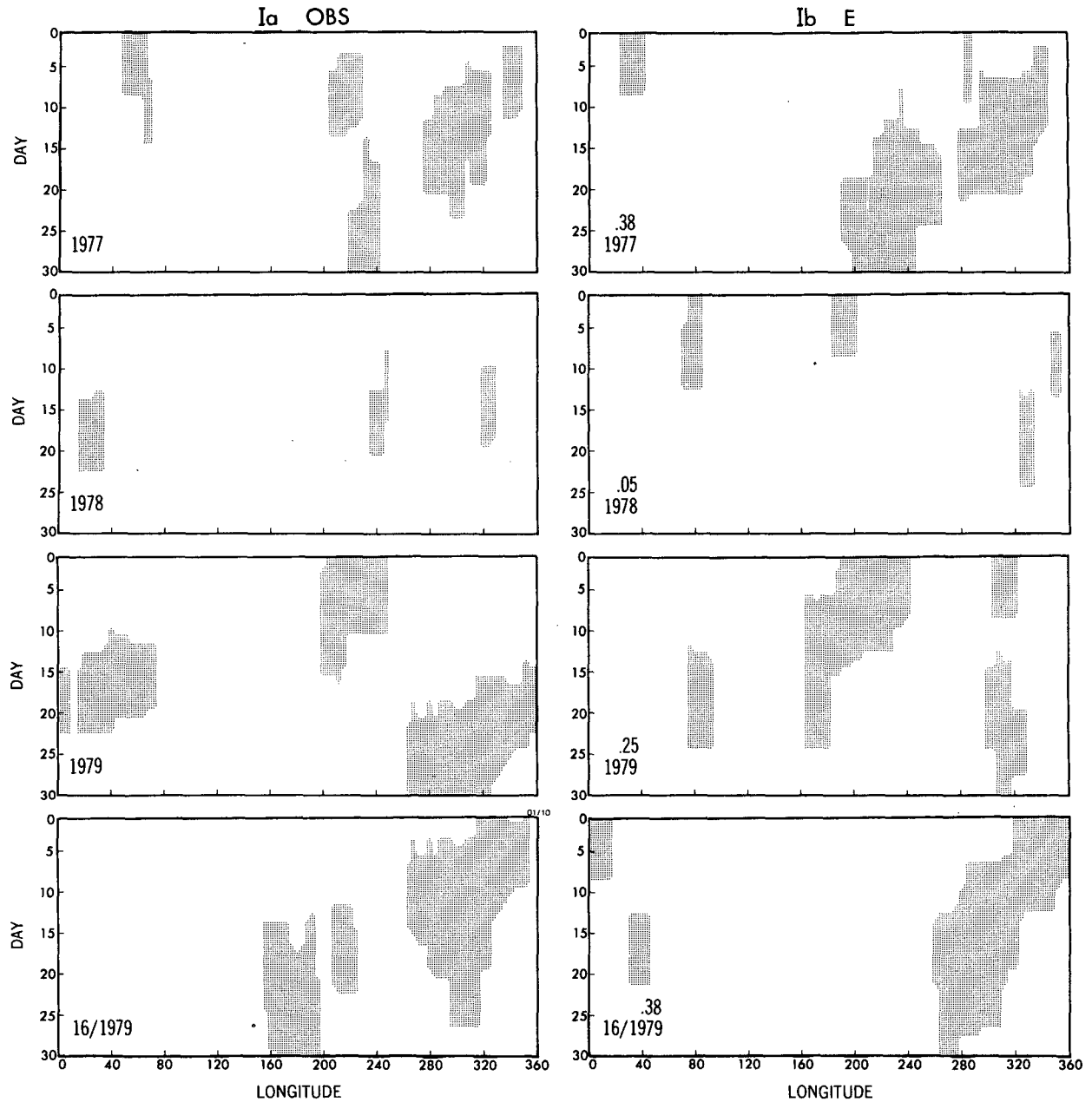| Cases	1977	1978	1979	1979(16)	1980	1981	1982	1983
Percentage area	14.3	4.0	21.8	21.0	22.7	34.0	12.0	15.5

FIG. 4. Comparison of the blocking signature between the observed (left) and the E-model (right) for four January cases. The threat scores are plotted at the lower left of each panel on the right hand side.

cerned with in this example are for the geopotential height at 500 hPa, but the discussion will be extended to other levels.

The failure/success of blocking forecasts is measured by the rating based on the threat and the bias scores of Method Ib together with the scores of Method Ia, using less weights for the latter. For example, the "worst" forecasts are selected as the cases of 1983, 1979 and 1981, based on the threat and bias scores, (0.18, 0.6), (0.25, 0.8) and (0.28, 0.5) for the three cases, respectively, in Method Ib, and (0.07, 0.1), (0.09, 0.2)

and (0.19, 0.2) in Method Ia. On the other hand, the "best" forecasts are: 1977, 1979(16) and 1982, based on the scores, (0.38, 1.0), (0.38, 0.8) and (0.13, 1.1) in Method Ib and (0.30, 0.5), (0.30, 0.3) and (0.13, 0.3) in Method Ia.

Figure 6 shows the forecast errors for 500 hPa geopotential height in the "best" and "worst" E-model forecasts. The error patterns of "worst," ΔZ_1, and "best," ΔZ_2, forecasts are the composites of three cases mentioned above and therefore, they are derived from nine 30-day forecasts for each case. These error patterns

TABLE 2. Threat scores for the blocking between the simulation and the observation. The left column uses Method Ia both for the verification and the forecasts (Ia:Ia) and the right column uses Method Ia for verification and Ib for the forecasts (Ia:Ib).

Model	Ia:Ia	Ia:Ib
A	0.11	0.20
E	0.15	0.23
F	0.12	0.23
FM	0.12	0.23

TABLE 4. Bias scores for the blocking between the simulation and observation. The left column uses Method IIa both for the verification and the forecasts (IIa/IIa) and the right column uses Method IIa for the verification and IIb for the forecasts (IIa/IIb).

Model	IIa/IIa	IIa/IIb
A	0.21	0.60
E	0.27	0.94
F	0.19	0.76
FM	0.23	1.11

are compared with the pattern of systematic error, ΔZ_E, of the E-model, which is virtually the same as that in Part I; the only difference is that the error in Fig. 6 is for Days 0–30, while the error in Part I is for Days 10–30.

Figure 6 reveals that the pattern in the upper left, ΔZ_1, resembles the systematic error pattern, ΔZ_E, in the upper right, while the pattern in the lower left, ΔZ_2, resembles, to a lesser extent, the systematic error, ΔZ_E. Table 5 is the result of a quantitative assessment of the similarity in terms of correlation coefficients between ΔZ_1 and ΔZ_E and between ΔZ_2 and ΔZ_E, and the root-mean-square differences $(\overline{(\Delta Z_1 - \Delta Z_E)^2}^H)^{1/2}$ and $(\overline{(\Delta Z_2 - \Delta Z_E)^2}^H)^{1/2}$, where $(\ )^H$ denotes the horizontal domain average for 90°–25°N. The table includes the verification not only of 500 hPa but also of other levels.

This table illustrates that the resemblance between ΔZ_1 and ΔZ_E is higher than that between ΔZ_2 and ΔZ_E, and that this relation holds for all levels in the troposphere. Besides the magnitudes of variation $(\overline{(\Delta Z)^2}^H)^{1/2}$, are largest in ΔZ_1, next ΔZ_E and smallest in ΔZ_2 (not shown here).

Thus Fig. 6 and Table 5 are not inconsistent to the finding of Tibaldi and Molteni; in their case, though, the blocking or the zonal flow episodes are classified by a very different criteria. Another important difference is that the correlation between ΔZ_2 and ΔZ_E in our case is not small, and the magnitude of error, ΔZ_2, is not small either, implying that the forecasts even in the "best" cases are not very good or that the systematic errors in our case are generated not only by the simulation of blocking, but also by other processes.

As discussed by Tibaldi and Molteni (1989), these error patterns can be divided into a zonally symmetric

part and an asymmetric part. The zonally symmetric part may be associated with the excessive cooling tendency of the model's atmosphere, in which the tendency is particularly strong at high latitudes (see Part I). The zonally asymmetric part is relevant to the misrepresentation of blocking.

To summarize the results in this subsection, a large portion of systematic error is associated with the failure of blocking forecasts, indicating that the errors in predicting "standing eddies" (the definition will be given in the next subsection, and also see Part I) are associated with blocking, and, as a result, the model's climatology deviates appreciably from reality.

b. Meridional distributions of kinetic energy

The horizontal distribution of kinetic energy (see Part I) may provide useful perspectives on the character of blocking. The kinetic energies are averaged over all vertical levels for the 24 runs of 30 days.

The upper panel of Fig. 7 for the zonal mean kinetic energy, K_M, reveals some aspects which are already known, such as the latitudinal shifts of the jet positions, compared with the observation. As will be discussed later, this deficiency appears to be critical for the blocking simulation. The lower panel for the eddy kinetic energy, K_E, exhibits a substantial underestimation of energy in the Southern Hemisphere, and to a lesser extent, in the Northern Hemisphere. The lack of K_E is almost synonymous with reduced blocking, and the zonality of flow.

Figure 8 is the decomposition of the eddy kinetic energy, K_E, into the standing (monthly mean) eddy
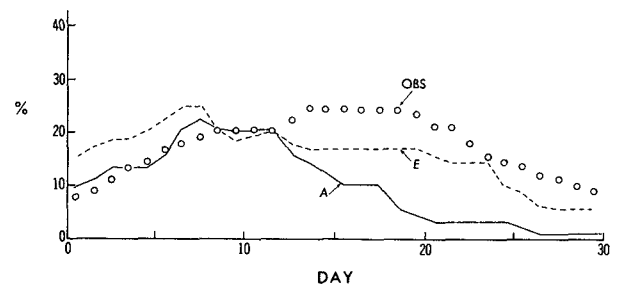
TABLE 3. The same as in Table 2, except the left column uses Method IIa both for the verification and the forecasts (IIa:IIa) and the right column uses Method IIa for the verification and IIb for the forecasts (IIa:IIb).

Model	IIa:IIa	IIa:IIb
A	0.05	0.21
E	0.08	0.30
F	0.07	0.30
FM	0.10	0.30

FIG. 5. Time evolutions of the blocking indices for the observation, the E- and the A-models. The abscissa is the forecasting time.

"worst" ΔZ_1

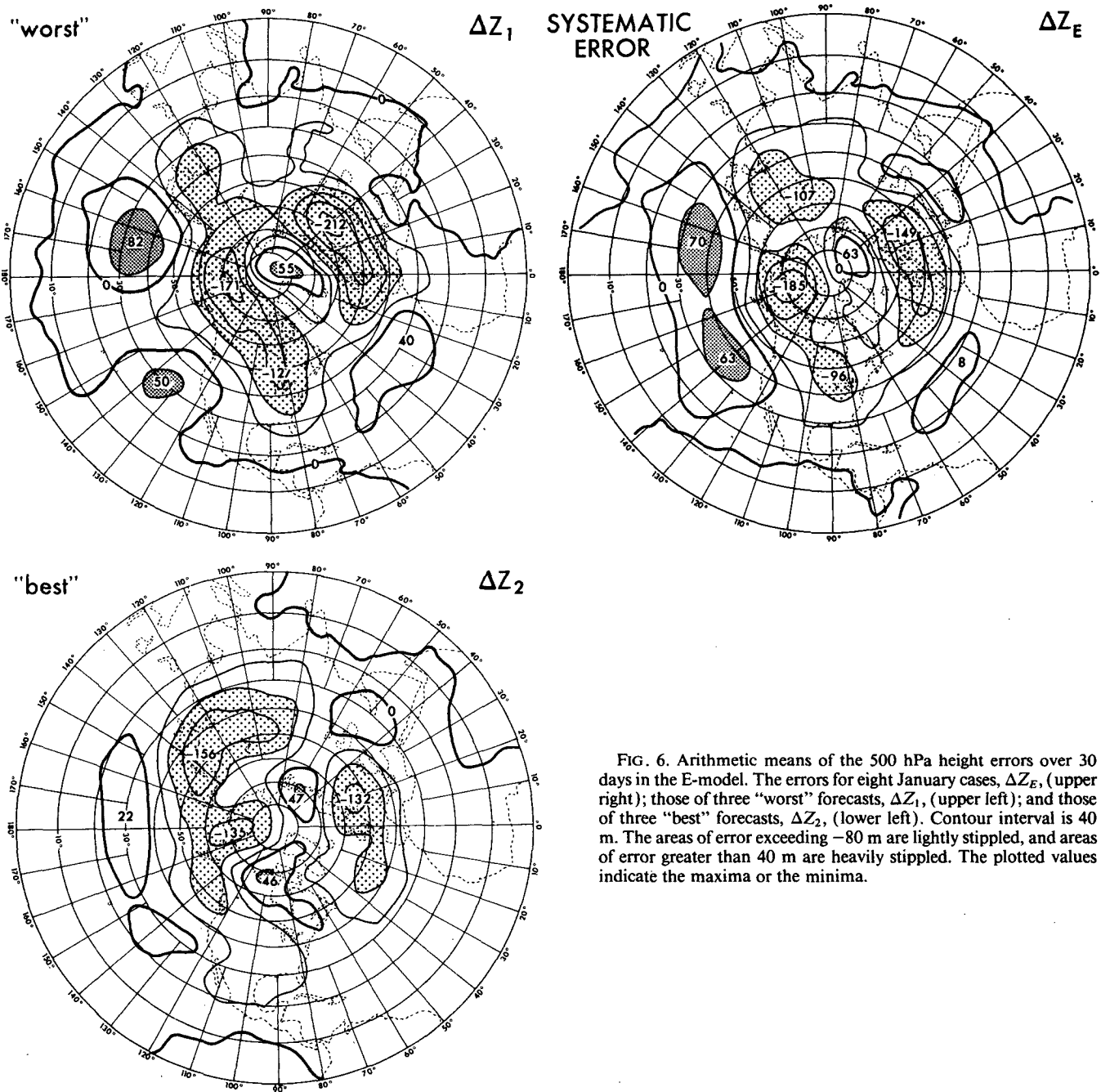SYSTEMATIC ERROR ΔZ_E

"best" ΔZ_2

FIG. 6. Arithmetic means of the 500 hPa height errors over 30 days in the E-model. The errors for eight January cases, ΔZ_E, (upper right); those of three "worst" forecasts, ΔZ_1, (upper left); and those of three "best" forecasts, ΔZ_2, (lower left). Contour interval is 40 m. The areas of error exceeding -80 m are lightly stippled, and areas of error greater than 40 m are heavily stippled. The plotted values indicate the maxima or the minima.

kinetic energy, K_{SE}, and the transient eddy kinetic energy, K_{TE} (see Part I). The averaging procedure is the same as for Fig. 7. For K_{SE} (upper panel) in the Northern Hemisphere, there are at least two maxima at latitudes of 35° and 55° (the third small peak is at tropics, i.e., 20°–10°N—see also Fig. 9). Attention is now called to a possibility that *the standing eddy kinetic energy at 55°N is related to blocking activities,* and the maximum consists mostly of zonal wavenumbers 1–3 with the center at 60°N (Tiedtke 1983).

The values for the FM are plotted only at selected latitudes by triangles, to avoid confusion with the other curves. As is seen in the upper panel, K_{SE} is represented better by the FM, the F and the E than by the A. It is interesting to note that the simulation is improved by increasing the mountain height from the F to the FM. Another interesting aspect is that the impact of the FM can be seen at 30°–50°S in the Southern Hemisphere.

Turning to the lower panel of Fig. 8, the transient eddy kinetic energy, K_{TE}, is appreciably underestimated

TABLE 5. The degrees of resemblance between the forecast error patterns and the systematic error patterns for various vertical levels are assessed by the correlation coefficients and the root-mean square errors.

hPa	Correlation coefficient		Rms difference (in meters)	
	$\Delta Z_1 : \Delta Z_E$	$\Delta Z_2 : \Delta Z_E$	$\sqrt{(\Delta Z_1 - \Delta Z_E)^2}$	$\sqrt{(\Delta Z_2 - \Delta Z_E)^2}$
200	0.83	0.73	41	47
300	0.84	0.63	39	51
400	0.84	0.61	35	47
500	0.86	0.64	30	40
700	0.89	0.71	23	29
850	0.89	0.75	20	24
1000	0.89	0.80	20	22

by all models, especially in the Southern Hemisphere. The magnitude of K_{TE} for the globe are, in descending order, the A, the E, the F and the FM consistently for all eight cases (not shown here). It is a point of argument whether the transient eddies are essential for the generation and maintenance of blocking. Yes, it is important (see Pierrehumbert and Malguzzi 1984; Illari
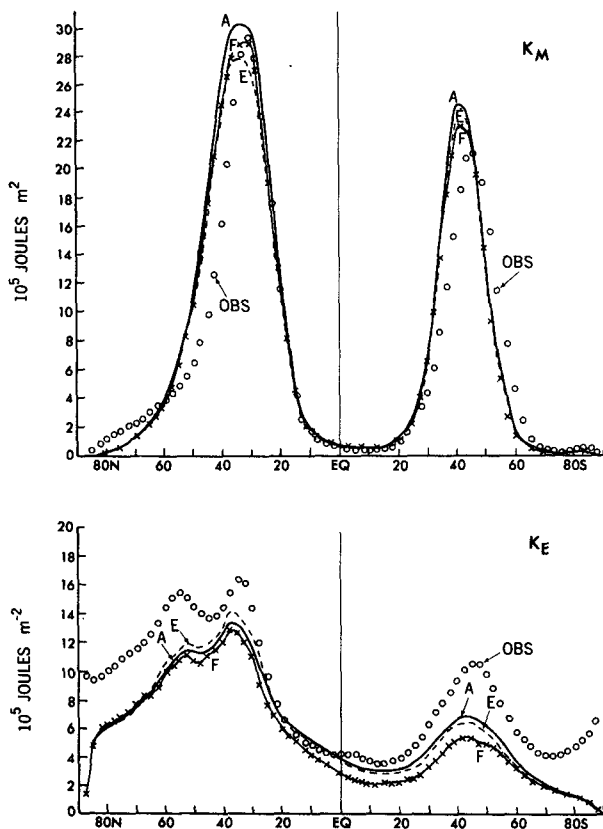

FIG. 7. Latitudinal distributions of zonal mean kinetic energy, K_M, and eddy kinetic energy, K_E; both are averaged vertically over a month. Small circles are observations. The A-model is indicated by thick solid line (——); the E-model by dashed line (- - -); and the F-model by thin solid line connected by crosses (-✕-✕-✕-).
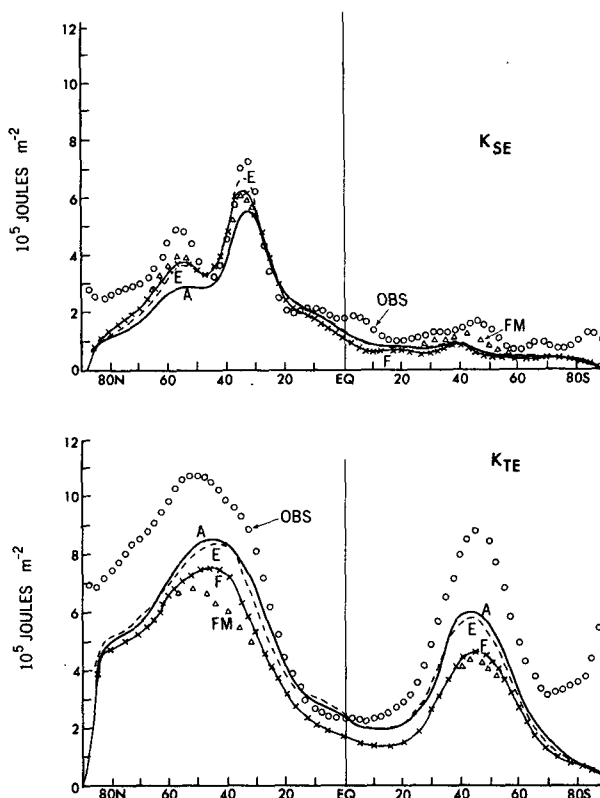

FIG. 8. As in Fig. 7 but for standing eddy kinetic energy, K_{SE}, and transient eddy kinetic energy, K_{TE}. Small triangles are for the FM-model.

1984); however, as is seen in the lower part of Fig. 8, the most successful case of blocking simulation (the FM-physics) produces the least amount of transient eddies, while the most unsuccessful case (the A-physics) produces the largest amount of transient eddies. From this fact, it may be stated that the amount of the transient eddies alone is not crucial for the successful model forecast of blocking.

c. *Remarks on the eddy kinetic energies*

The upper panel of Fig. 8 depicts the latitudinal distribution of K_{SE}. Similar distributions of the observed K_{SE} are shown by Oort (1983), Lau and Oort (1981) and Oriol (1982) together with other relevant variables. Figure 9 is the K_{SE} obtained by Oort (1983) for January and February based on 15 years of data. The subpolar (55°) peak of energy is unmistakably evident. This energy peak (55°N) consists mostly of the meridional component of the wind, i.e., $\frac{1}{2}[\overline{v^*}^2]$ (Fig. 10b), while the midlatitude (30°N) peak consists mostly of the zonal component, i.e., $\frac{1}{2}[\overline{u^*}^2]$ (Fig. 10a). Here [ ] denotes the zonal mean; ( )* is the eddy component which is the deviation from the zonal mean; and (̄) is the monthly mean (see Part I). It may also be informative to point out (not shown here) that the
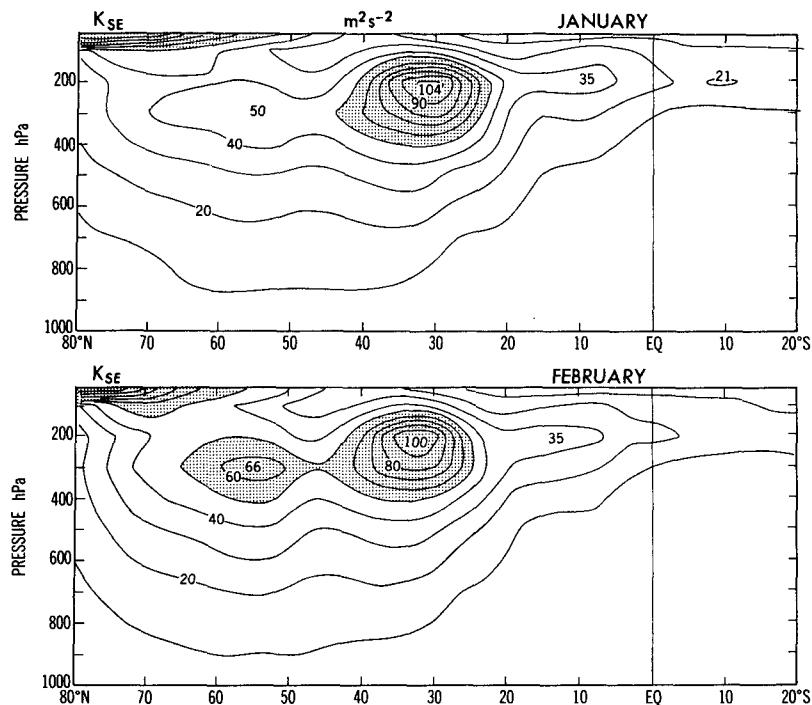
FIG. 9. The standing eddy kinetic energies, K_{SE}, in the latitude–pressure diagrams. The upper panel is for January and the lower panel is for February. Contour interval is 20 m^2 s^{-2}. The areas whose values are greater than 60 m^2 s^{-2} are stippled (after Oort 1983).

standing (time-mean) eddy variances of geopotential height, $[\overline{z^*}^2]$, and of temperature, $[\overline{T^*}^2]$, have the peaks immediately south of the central position of K_{SE}, and that the poleward heat flux, $[\overline{vT}]$ (standing and transient), exhibits its maximum at these latitudes, and $[\overline{u^*v^*}]$ changes its sign around this latitude, suggesting an appreciable amount of convergence of low-frequency eddy momentum. For these reasons, the 55°N peak has a particular significance in the eddy activities of the atmosphere, and especially the large-scale wave components of low frequency are involved in this peak. Perhaps it is most important in our experiment to note that *the E, the F and the FM in Fig. 8 reproduce the subpolar peak well, compared with the A*. This feature appears to be related to the good performance of the E and the F in the earlier period of 1-month forecast (see Fig. 10 and Fig. 11 in Part I), and the smaller forecast errors (see Fig. 5 in Part I).

Concerning the drawbacks in the simulation of K_{TE}, many candidates for the error sources can be listed, such as the insufficient spatial resolution of the GCM, the insufficient amount of heat release in the low latitudes, the excessive vertical and lateral diffusion, and inadequate cumulus parameterization. The reasons why the A and the E are better than the F and the FM in the production of K_{TE} may be 80% condensation criterion in the former instead of 100% in the latter,

and also the moist convective adjustment, compared with the "penetrative" convection parameterization by the A–S (Arakawa–Schubert) scheme. This was indeed the rationale for the adoption of 80% criterion, although admittedly there is an associated drawback discussed in Part I.

The reduction of K_{TE} in the FM from the F is consistent with the GCM experiment of Manabe and Terpstra (1974), and Hayashi and Golder (1983), although the variation of orography in their experiments are rather extreme, i.e., with and without mountains. One of their conclusions (Hayashi and Golder 1983) is that, in the presence of mountain, the eastward moving planetary waves are decreased in amplitude, while the westward moving waves are increased. In particular, the eastward waves of zonal wavenumber 2–6 for the period of 7–20 days, and the westward waves of zonal wavenumber 1–3 for the same period are affected appreciably by the orography. From the standpoint of blocking simulation, this situation appears favorable, i.e., suppressing the erroneous eastward moving waves and enhancing the weak westward moving waves [for the Pacific block, at least—see Tibaldi and Molteni (1989)]. The only shortcoming of the enhanced mountain, such as the FM, however, is that the "good" performance in terms of forecast score (Part I) has been achieved at the sacrifice of transient eddy components.
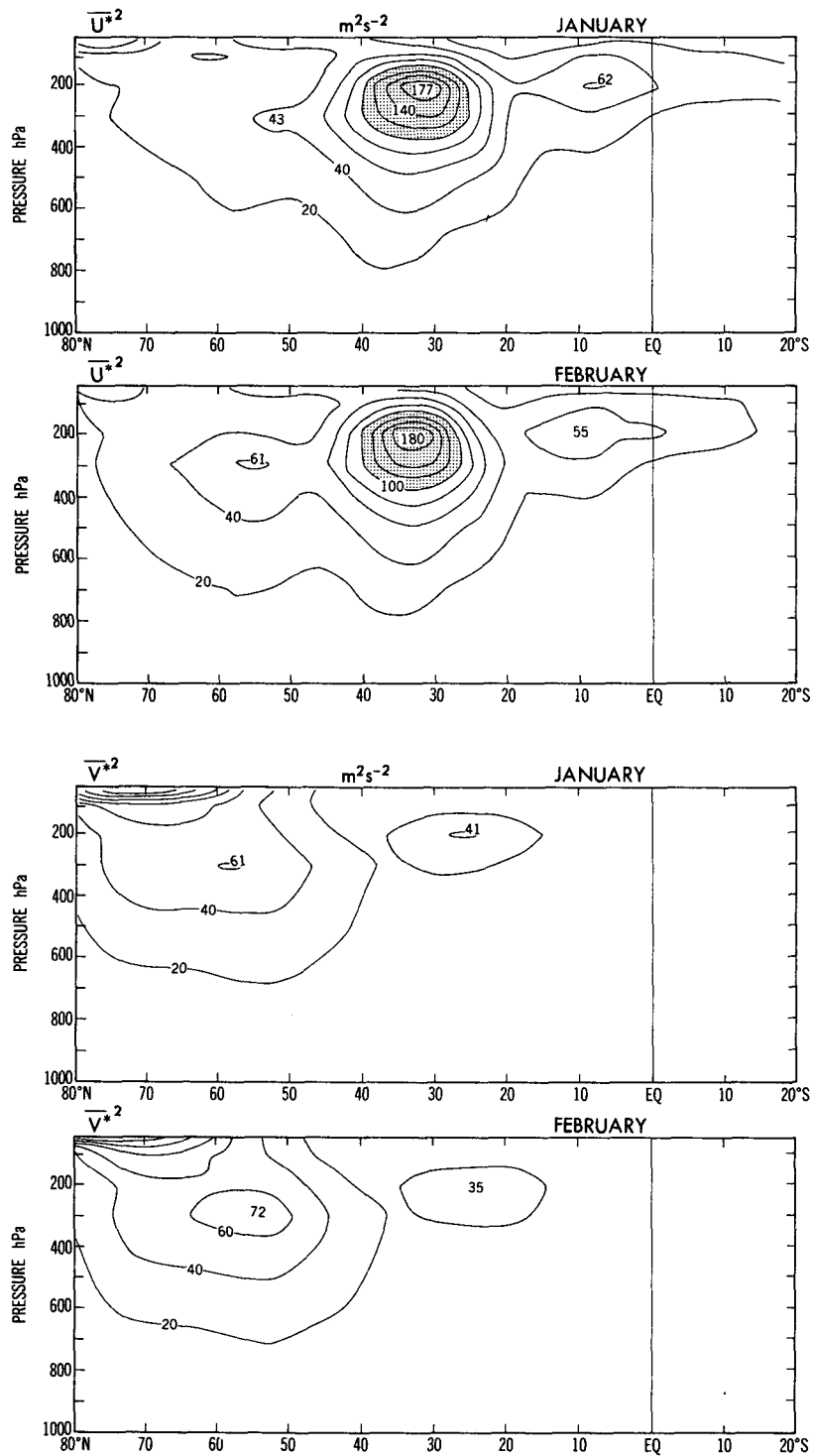
FIG. 10. Each component of standing eddy kinetic energies for January (upper) and February (lower). Panel (a) is for $[u^{*2}]$ and panel (b) is for $[v^{*2}]$. Contour interval is 20 m^2 s^{-2} (after Oort 1983).

d. The subpolar peak of low-frequency eddy kinetic energy

Figure 11 shows the results of the zonal mean kinetic energy, K_M, (left), and the standing eddy kinetic energy, K_{SE}, (right), in the most successful (upper) and the most unsuccessful (lower) cases of blocking forecasts by the E-model. The plotted values at the upper right corner of K_{SE} are the threat and the bias scores in Method Ib.

It may be seen in K_{SE} (right) that the successful forecasts of blocking give well-defined subpolar peaks of standing eddies, while the failing cases have ill-defined peaks. Correspondingly, the distributions of K_M (left) are such that in the unsuccessful cases K_M in the model tends to extend poleward, compared with the observational counterpart.

In this connection, the study of Nigam and Lindzen (1989) is intriguing. They calculate the orographically forced stationary waves using a high-resolution steady linear primitive equation model and specified zonally symmetric basic flows. The study suggests a remarkable sensitivity of stationary wave amplitudes to small latitudinal shifts in the location of the subtropical jet. Figure 12 shows the meridional distribution of K_M (top panel, $[\bar{v}] = 0.0$ in their case) and K_{SE} (bottom panel)
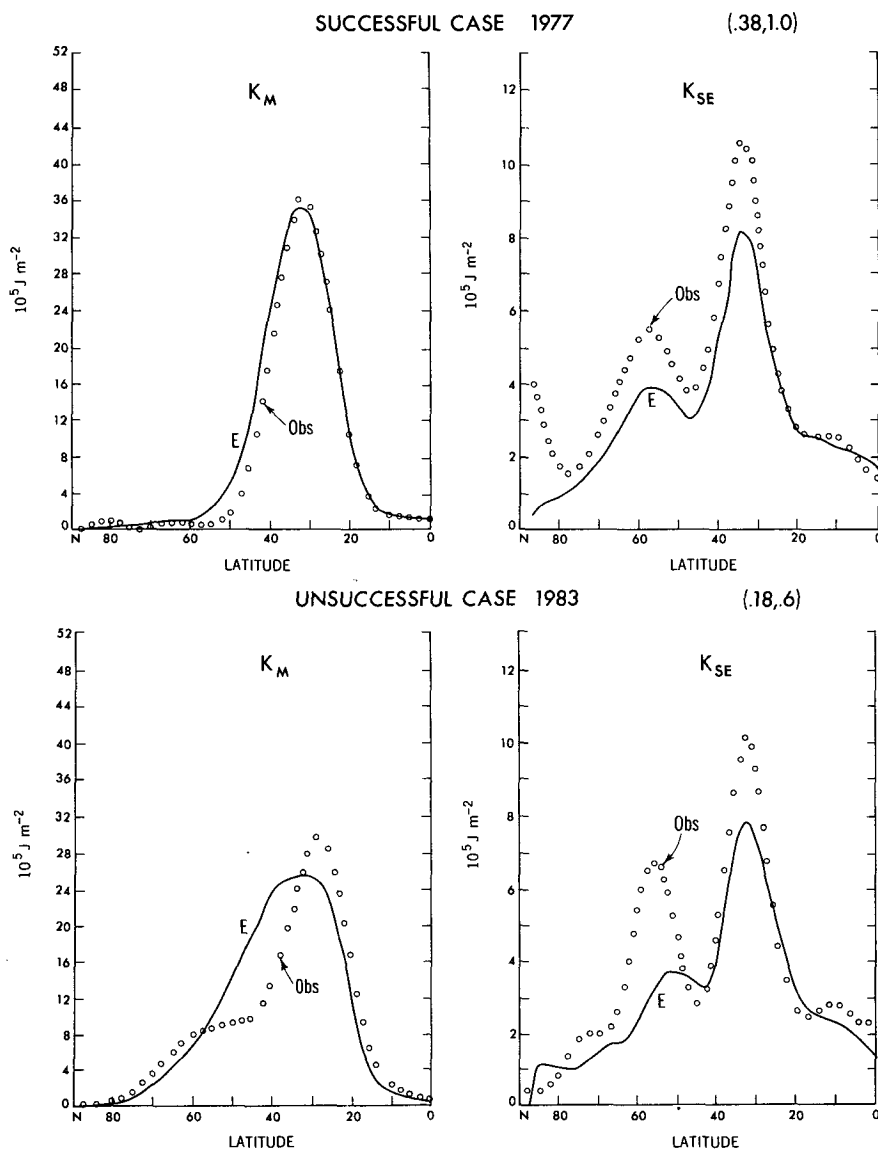

FIG. 11. Latitudinal distribution of zonal mean kinetic energy, K_M, (left) and standing eddy kinetic energy, K_{SE}, (right), for the successful case (upper) of blocking forecast, and for the unsuccessful case (lower). The figures in the parentheses (a, b) indicate the threat (a) and bias (b) scores.
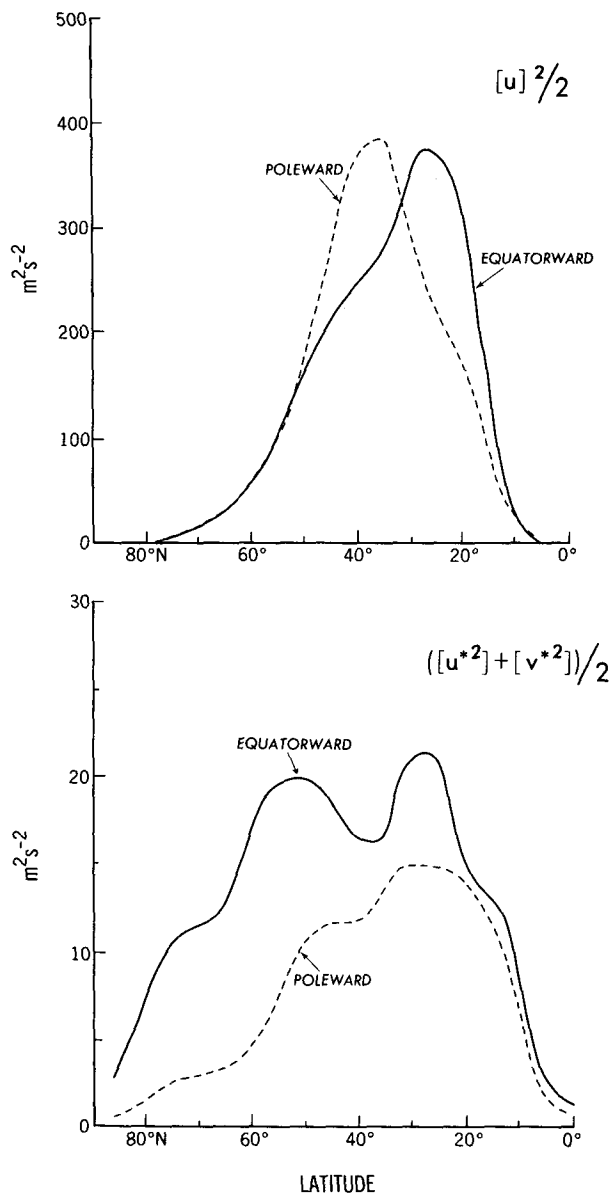
FIG. 12. Latitudinal distributions of zonal mean wind square, $[u]^2/2$, (upper) and of the standing eddies, $([u^{*2}] + [v^{*2}])/2$, (lower), for the two situations, i.e., the poleward and the equatorward positioned jets. (Courtesy of Nigam and Lindzen.)

at the 500 hPa level for two cases: an equatorward and a poleward shift of the subtropical jet about its mean position (corresponding to Figs. 9a and 9b in their paper). The 55°N peak is stronger in the case of the equatorward shifted jet. Nigam and Lindzen explain the sensitivity of solutions in terms of changes in the stationary wave refractive index which in turn affect wave propagation in the meridional and vertical. The equatorward-displaced subtropical jet, in their picture, effectively deflects more stationary wave energy poleward, leading to the enhanced tropospheric and strato-

spheric stationary waves in the subpolar latitudes of the western hemisphere. Although the ratio of K_{SE} to K_M in Fig. 12 is low compared with the observed ratio (in part, because only orographic forcing is considered in their study), Fig. 12 suggests that the latitudinal position of subtropical jet or the meridional profile of the jet is an element of consequence for blocking activities, and that this aspect should be further pursued within the framework of GCM simulations.

4. The E- versus the A-models

a. Performance differences

As was discussed earlier, the superiority of the E-model over the A-model is seen in the standing eddy kinetic energy, K_{SE}. Studies of energetics associated with blocking have been performed extensively in the 1960s and 1970s. Several papers have appeared even after 1977, for example, Lejenäs (1977), Holopainen (1978), Chen et al. (1981), Hansen and Chen (1982), Hansen and Sutera (1984), Kung and Baker (1986), and Lee and Chen (1986). All studies indicate that both barotropic and baroclinic processes are involved in generating K_{SE}, though the degree of conversion from potential to kinetic energy and the feature of up-scale cascade in kinetic energy are different with respect to the cases and the development stages of blocking. Based on these studies it is speculated that the potential capability of nonlinear interaction is not vastly different between the E-model and the A-model, but the feature of baroclinic conversion is different from each other and is more favorable for the subpolar peak of K_{SE} in the E-model than in the A-model.

In order to discuss the 50°N peak of K_{SE}, the conversion $[-\bar{\omega}^*\bar{\alpha}^*] = C(A_{SE}, K_{SE})$ (see Hansen et al. 1984) is required, where ω is the vertical pressure velocity, α is the specific volume, ( )* is the deviation from the zonal mean (eddy), and ( )* is the standing eddy. It is interesting to note that, as shown in Miyakoda and Sirutis (1983), the conversion rate from the total eddy available potential energy, A_E, to the total eddy kinetic energy, K_E, i.e., $[-\omega^*\alpha^*] = C(A_E, K_E)$ is, in the descending order, the A, the E and the F. The E-model contains vertical turbulent transfer processes which diminish $C(A_E, K_E)$ due to larger static stability, and the F-model has the penetrative cumulus convection process, which leads to even smaller magnitudes of $C(A_E, K_E)$. This fact may account for why the total eddy kinetic energy K_E, and therefore the transient energy, K_{TE}, are in the descending order, the A, the E and the F. $C(A_{SE}, K_{SE})$, however, is different from $C(A_E, K_E)$ (not shown here); it is in the descending order, the F, the E and the A.

To summarize the above, there are two major issues in the error associated with the model's blocking simulation, i.e., first, the systematic bias in the pole-to-equator temperature gradient and accordingly, the excessively intense zonal flow, and second, the model's

behavior in terms of standing eddy activities especially at the exit of storm tracks. The first issue is extremely important, because the strong zonal flow tends to break the blocking regime more easily. But as was discussed in Part I, this problem is too difficult to solve immediately, because the radiation processes and the spatial resolution may be involved. In this paper, putting aside the first issue, we make the following point. *It is likely that the E-model produces more favorable distributions of standing eddies (probably through the longitudinally coherent phase relation between ω^* and $\overline{\alpha^*}$) at about 55°N, compared with the A, so that the subpolar peak in K_{SE} is better reproduced by the E than the A.*

b. Vertical turbulent transfer processes

If the understanding and reasoning mentioned in the previous subsection are correct, the next question may be how the favorable conditions for the blocking are produced in the E. Turning to the difference of SGS physics between the A- and the E-models, it can be stated that the incremental components of the E beyond the A are the turbulence closure scheme, the Monin–Obukhov boundary layer physics, and the subsurface soil heat conduction. Of these three physics, which one is most relevant and accordingly responsible for the better representation of blocking? In order to examine whether the difference comes from the turbulence closure scheme or the Monin–Obukhov scheme or the turbulent length-scale, two additional experiments are carried out by transplanting two different features of the A-model into the E-model.
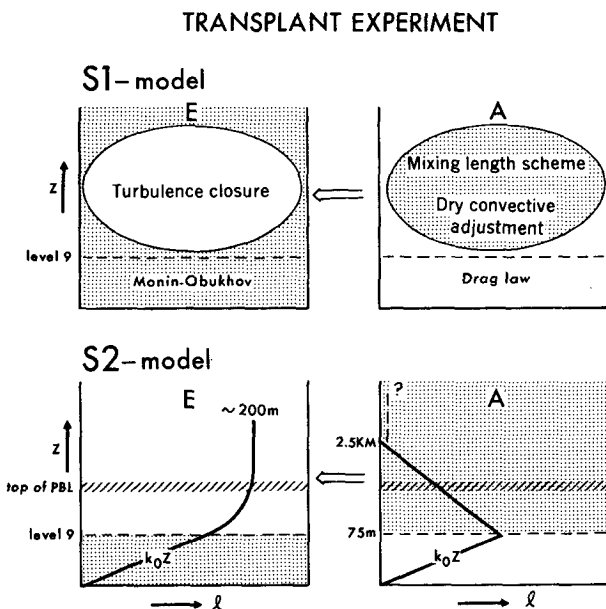
TRANSPLANT EXPERIMENT

FIG. 13. Illustration of S1- and S2-model, which are used in the transplant experiments.
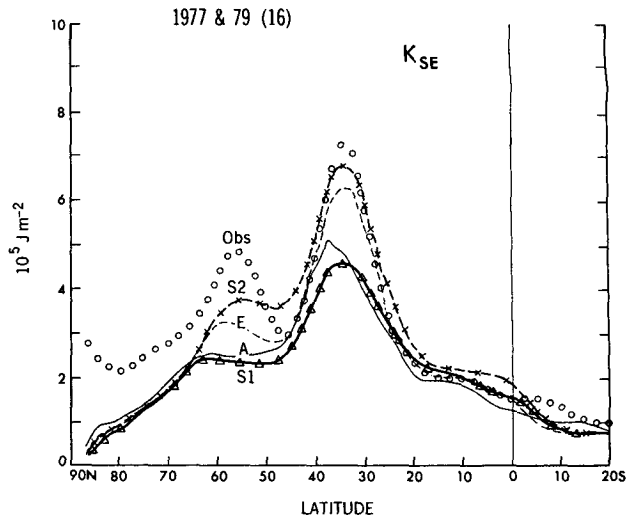

FIG. 14. Latitudinal distributions of standing eddy kinetic energy, K_{SE}, for the combined cases of 1977 and 1979(16) by the four models, the S1-, the S2-, the E- and the A-models, and the observation.

1) THE S1-MODEL

Using the E-model as the base, a special model, S1, is designed by transplanting the turbulent flux parameterization of the A-model into the layer above the lowest level (level 9). Namely the turbulence closure scheme in the E is now replaced by the "mixing length" scheme for momentum and the dry convective adjustment for temperature (see the upper part of Fig. 13).

2) THE S2-MODEL

For the investigation of whether the turbulent mixing length-scale is the key cause of the difference, a special model is designed (see the lower part of Fig. 13). In the A-model, the turbulent diffusion is performed using a turbulent length-scale, l, which has a maximum at the level of 75 m, decreases with height, and becomes zero above the 2.5 km level (Smagorinsky et al. 1965), while the E has the length-scale asymptote to a constant value (about 200 m) above the ninth level. This indicates that the A-model has no vertical diffusion in upper troposphere above 2.5 km, except the dry adiabatic adjustment. Between 2.5 km and the ninth level, the vertical diffusion in the A is performed only for momentum through the mixing length scheme, using the turbulent length-scale described above. In the S2-model, the similar distribution of the length-scale to the A is used with other features of the E unchanged.

These models, the S1 and S2, are applied to two January cases, i.e., 1977 and 1979(16). The results of the tests are displayed in Figs. 14, 15 and 16. Figure 14 is the latitudinal distribution of standing eddy kinetic energy, K_{SE}. The figure indicates that, the S1-model behaves similarly to the A-model, while the S2-
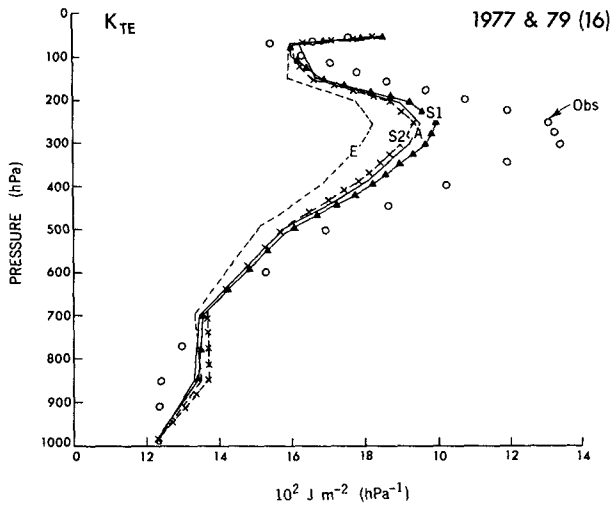
FIG. 15. Vertical distributions of transient eddy kinetic energy, K_{TE}, for the combined cases of 1977 and 1979(16) by the four models, the S1-, the S2-, the E- and the A-models, and the observation. The domain is the globe.

model gives similar results to or even better results than the E-model. This implies that the reason why the E outperforms the A appears to be neither the Monin–Obukhov process nor the turbulent length-scale à la E-model, but the turbulence closure scheme.

Figure 15 shows that the S1-model gives larger amounts of transient eddies than the E and the A-models, and that the S1-model gives larger transient than the S2-model. In other words, the turbulence closure scheme tends to suppress the transient, while it generates more standing eddies. It appears that the turbulent length-scale à la E-model is not desirable. We will come back to this point later. Figure 16 shows the forecasting skill scores of 10 day mean 500 hPa height in terms of the anomaly correlation coefficient and the root-mean-square errors. These diagrams indicate that the skill scores are similar between the E and the S2 and between the A and the S1, respectively. The fact confirms the point that the superiority of the E over the A is not the Monin–Obukhov process but the turbulence closure scheme. Perhaps the present experiment is the first to demonstrate the merit of the level 2.5 turbulence closure scheme outside of the planetary boundary layer. Note, however, that it is not clear whether the level 2 closure (stability-dependent vertical diffusion) is sufficient instead of the level 2.5 closure [see Mellor and Yamada (1982) for the definitions of level 2 and 2.5 closure].

It is a by-product to know that the turbulent length-scale in the A-model type is more desirable for enhancing transient eddies and even enforcing the 55°N peak of standing eddies, though the skill scores are not necessarily raised. More detailed investigation reveals that a small positive value of l rather than absolute zero above 2.5 km is even better. Recently the ECMWF

has mentioned that their parameterized vertical diffusion for momentum is too strong in the free atmosphere above the planetary boundary layer. Based on this result, the revised version of their operational model has zero diffusion above the boundary layer since January 1988 (Klinker and Sardeshmukh 1988), though this change may have been too drastic.

One of the shortcomings in the current theory of turbulence closure is that the specification of the turbulent length-scale, l, is theoretically not well founded (Mellor and Yamada 1982). In an ocean simulation study of the Equatorial Undercurrent during an El Niño, it was found that the length-scale, l, should be extremely small (but not zero) beneath the thermocline (Rosati and Miyakoda 1988) to obtain a good simulation of the undercurrent. This is another example of the need for either empirical correction of the length-scale distribution, or a firmer theoretical basis for its magnitude.
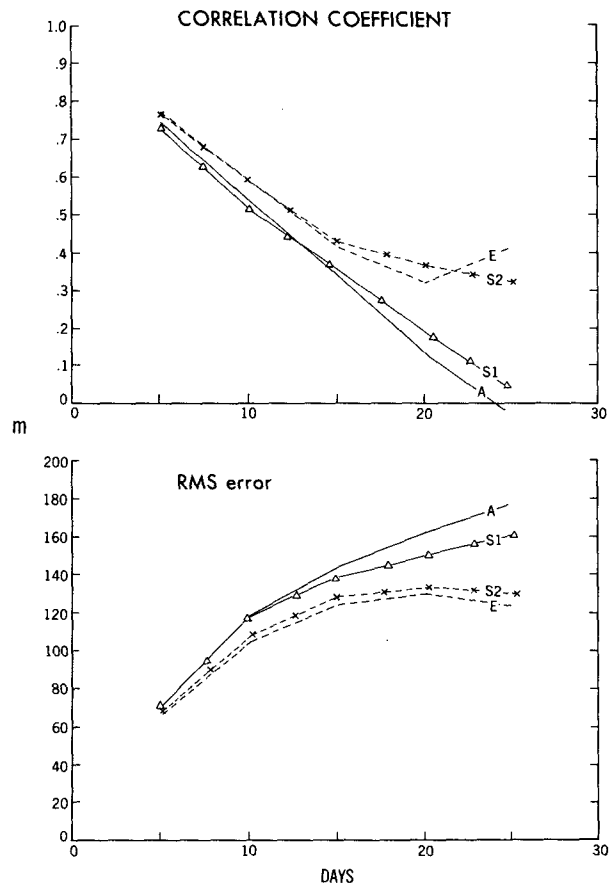

FIG. 16. The correlation coefficients (upper) of 10 day mean of 500 hPa geopotential height anomalies between the forecasts and the observation for the combined cases of 1977 and 1979(16). The root-mean-square forecast errors (lower) of 10 day mean of 500 hPa geopotential height for the combined cases of 1977 and 1979(16). The verification domain is 90°–25°N in the Northern Hemisphere.

5. Hypothesis on the meridional position of the mid-latitude jet

Dole (1986) presented a detailed synoptic description of the evolution of blocking. Among the many features described, one aspect relevant to the present discussion is that, in the case of Pacific blocking, the zonal wind in the southwestern Pacific strengthens prior to the onset, and the zone of intense jet stretches eastward (not northeastward) near 160°E. Associated with this jet, low pressure anomalies start to leave the jet exit, develop explosively around the date line, and simultaneously move northward. East of this developing low, a strong high emerges, which subsequently becomes the blocking high. Lau's (1981) statistical assessment of his 15 year GCM run is consistent with some aspects of this picture. He showed that the meridional positions of the jetstream axes are distinctly different in two circulation regimes, i.e., the M+ (the blocked) and the M− (the zonal flow) cases. The jet axes in the blocked case are located south of those in the zonal flow case by as much as 10° of latitude; the intensity at the core is stronger by 5 m s^{-1} at the 500 hPa level; interestingly enough, the westerlies at 40°N–60°N are extremely weak or even negative in the blocked case. Shutts (1986), Hoskins and Sardeshmukh (1987) and Haines and Marshall (1987) made analyses of potential vorticity, using the operational weather maps. Hoskins (1988) summarized these observations on the formation of blocking high: "The major ingredient of a blocking high is the low potential vorticity; this vorticity is typical of a latitude 20° or so near the equator; and the poleward movement of subtropical air with its low vorticity into the mean anticyclonic region is evident." See also Mahlman (1979) for a similar argument, i.e., the importance of advection of warm air, low potential vorticity air from lower latitudes in sustaining a block.

This evidence, together with the discussion in subsection 3d, leads to a hypothesis that, in order to have blocking, *the jet axis prior to the onset has to be located at a relatively lower latitude.*

A question may be raised on the hypothesis: Is the weak westerlies in the upstream still valid (Hartmann and Gahn 1980)? The answer is yes, but the weak westerlies and the equatorward positioned jet are probably simultaneous features. The jet-axis is located south of 30°N at the early stage, and then the "modon" pattern is produced at high latitude; at this stage the westerlies west of the blocking at high latitudes (56°N–60°N—Treidl et al. 1981) should be weak.

Thus, the importance of the meridional position of the jet is reemphasized here. It is certain that the E-model is not entirely satisfactory in providing the correct latitudinal position of the jet or desirable meridional profile of jet. Even the FM-model is not satisfactory either.

Recently new parameterizations of "orographic gravity wave drag" have been used (see Part I). Although this problem is outside of the scope of the present study, the existing gravity wave drag methods do not appear to provide the necessary breakthrough for the improvement of blocking simulations.

6. Conclusions

The main points to emerge from this study are as follows:

(i) One of the outstanding features in monthly mean (standing) eddy kinetic energy, K_{SE}, for January in the Northern Hemisphere is the presence of two peaks in the latitudinal distribution of K_{SE}. One of them, located at about 55°N, is associated with blocking activity.

(ii) The simulation capability of blocking is appreciably enhanced by the E-model, compared with the A-model. This fact was found by investigation of two blocking indices with respect to the daily geopotential height maps.

(iii) The major factor for this improvement in (ii) is the turbulence closure scheme at the hierarchy level 2.5.

(iv) The capability of blocking simulation is also manifested by the well-defined peak of standing eddy kinetic energy at 55°N–60°N and the weak westerlies at 40°N–55°N west of the blocking ridge. The F, the FM and the E-models represent this subpolar peak better than the A-model.

(v) A hypothesis is proposed: In order to have a blocking, the jet axis prior to the onset has to be located at relatively lower latitudes.

(vi) A large portion of systematic error comes from the failure of blocking forecasts, supporting the finding of Tibaldi and Molteni (1988).

(vii) As far as the turbulent length-scale is concerned, the vertical distribution specified in the conventional A-model is more desirable than that included in the recent E-model. Namely, the length-scale should be zero or small value above 700 hPa level.

REFERENCES

Arpe, K., 1988: Planetary-scale diabatic forcing errors in the ECMWF model. *ECMWF Workshop on "Diabatic Forcing,"* Reading, Berkshire, England, 103–150.

Blackmon, M. L., S. L. Mullen and G. T. Bates, 1986: The climatology of blocking events in a perpetual January simulation of a spectral general circulation model. *J. Atmos. Sci.,* **43,** 1379–1405.

Chen, T.-C., A. R. Hansen and J. J. Tribbia, 1981: A note on the

release of available potential energy. *J. Meteor. Soc. Japan,* **59,** 355–359.

Dole, R. M., 1986: The life cycles of persistent anomalies and blocking over the North Pacific. *Adv. Geophys.,* **29,** 31–69.

——, and N. D. Gordon, 1983: Persistent anomalies of the extratropical Northern Hemisphere wintertime circulation: Geographical distribution and regional persistence characteristics. *Mon. Wea. Rev.,* **111,** 1567–1586.

Hansen, A. R., and T.-C. Chen, 1982: A spectral energetics analysis of atmospheric blocking. *Mon. Wea. Rev.,* **108,** 1146–1165.

——, and A. Sutera, 1984: A comparison of the spectral energy and enstrophy budgets of blocking versus nonblocking periods. *Tellus,* **36A,** 52–63.

Hartmann, D. L., and S. J. Ghan, 1980: A statistical study of the dynamics of blocking. *Mon. Wea. Rev.,* **108,** 1144–1159.

Hayashi, Y., and D. G. Golder, 1983: Transient planetary waves simulated by GFDL spectral general circulation models. Part I: Effects of mountains. *J. Atmos. Sci.,* **40,** 941–950.

Hollingsworth, A., U. Cubasch, S. Tibaldi, C. Brankovic, T. N. Palmer and L. Campbell, 1987: Mid-latitude atmospheric prediction on time scales of 10–30 days. *Atmospheric and Oceanic Variability,* Cattle, Ed., *Roy. Meteor. Soc. Monograph,* 117–151.

Holopainen, E. O., 1978: A diagnostic study on the kinetic energy balance of the long-term mean flow and the associated transient fluctuations in the atmosphere. *Geophysica,* **15,** 125–145.

Hoskins, B. J., 1988: Theories of blocking. *ECMWF Seminar Proceedings on The Nature and Prediction of Extra-Tropical Weather Systems,* Volume II, Reading, Berkshire, England, 1–10.

——, and P. D. Sardeshmukh, 1987: A diagnostic study of the dynamics of the Northern Hemisphere winter of 1985–86. *Quart. J. Roy. Meteor. Soc.,* **113,** 759–778.

Illari, L., 1984: A diagnostic study of the potential vorticity in a warm blocking anticyclone. *J. Atmos. Sci.,* **41,** 3518–3526.

Klinker, E., and P. D. Sardeshmukh, 1988: The diagnosis of systematic errors in numerical weather prediction models. *ECMWF Workshop on Diabatic Forcing,* Reading, Berkshire, England.

Knox, J. L., and J. E. Hay, 1985: Blocking signatures in the Northern Hemisphere: Frequency distribution and interpretation. *J. Climate,* **5,** 1–16.

Kung, E. C., and W. E. Baker, 1986: Spectral energetics of the observed and simulated Northern Hemisphere general circulation during blocking episodes. *J. Atmos. Sci.,* **43,** 2792–2812.

Lau, N.-C., 1981: A diagnostic study of recurrent meteorological anomalies appearing in a 15-year simulation with a GFDL general circulation model. *Mon. Wea. Rev.,* **109,** 2287–2311.

——, and A. H. Oort, 1981: A comparative study of observed northern hemisphere circulation statistics based on GFDL and NMC analyses. Part I: The time-mean fields. *Mon. Wea. Rev.,* **109,** 1380–1403.

Lee, Y.-H., and T.-C. Chen, 1986: Structure and energetics of standing eddies in the winter Northern Hemisphere simulated by the NCAR Community Climate Model and the GLA climate model. *Mon. Wea. Rev.,* **114,** 2057–2077.

Lejenäs, H., 1977: On the breakdown of the westerlies. *Atmosphere,* **15,** 89–113.

——, and H. Økland, 1983: Characteristics of Northern Hemisphere blocking as determined from a long time series of observational data. *Tellus,* **35A,** 350–362.

Mahlman, J. D., 1979: Structure and interpretation of blocking anticyclones as simulated in a GFDL general circulation model. *Proceedings of the Thirteenth Stanstead Seminar,* Publication in *Meteorology,* No. 123, T. Warn, Ed., Dept. of Meteorology, McGill University, pp. 70–76.

Manabe, S., and T. B. Terpstra, 1974: The effects of mountains on the general circulations of the atmosphere as identified by numerical experiments. *J. Atmos. Sci.,* **31,** 3–42.

Mansfield, D. A., 1986: The skill of dynamical long-range forecasts, including the effect of sea surface temperature anomalies. *Quart. J. Roy. Meteor. Soc.,* **112,** 1145–1176.

McWilliams, J. C., 1980: An application of equivalent modons to atmospheric blocking. *Dyn. Atmos. Ocean,* **5,** 43–66.

Mellor, G. L., and T. Yamada, 1982: Development of a turbulence closure model for geophysical fluid problems. *Rev. Geophys. Space Phys.,* **20,** 851–875.

Miyakoda, K., and J. Sirutis, 1983: Impact of subgrid-scale parameterizations on monthly forecasts. *ECMWF Workshop on Convection in Large Scale Models,* Reading, Berkshire, England, pp. 231–277.

——, —— and J. Ploshay, 1986: One-month forecast experiments—without anomaly boundary forcings. *Mon. Wea. Rev.,* **114,** 2363–2401.

——, T. Gordon, R. Caverly, W. Stern, J. Sirutis and W. Bourke, 1983: Simulation of a blocking event in January 1977. *Mon. Wea. Rev.,* **111,** 846–869.

Nigam, S., and R. S. Lindzen, 1989: The sensitivity of stationary waves to variations in the basic state zonal flow. *J. Atmos. Sci.,* **46,** 1746–1768.

Oort, A. H., 1983: *Global atmospheric circulation statistics.* NOAA Prof. Paper No. 14, Rockville, MD 20852, 180 pp.

Oriol, E., 1982: Energy budget calculations at ECMWF. Part I. Analyses 1980–81. ECMWF Tech. Rep., No. 35, 111 pp. [Available at European Centre for Medium-Range Weather Forecasts, Springfield Park, Reading, Berkshire, RG2, 9AX, England.]

Pierrehumbert, R. T., and P. Malguzzi, 1984: Forced coherent structures and local multiple equilibria in a barotropic atmosphere. *J. Atmos. Sci.,* **41,** 246–257.

Rex, D., 1950: Blocking action in the middle troposphere and its effect upon the regional climate. I. An aerological study of blocking action. *Tellus,* **2,** 196–211.

Rosati, A., and K. Miyakoda, 1988: A general circulation model for upper ocean simulation. *J. Phys. Oceanogr.,* **18,** 1601–1626.

Sanders, F., and J. R. Gyakum, 1980: Synoptic–dynamic climatology of the "bomb." *Mon. Wea. Rev.,* **108,** 1589–1606.

Shukla, J., and K. C. Mo, 1983: Seasonal and geographical variations of blocking. *Mon. Wea. Rev.,* **111,** 388–402.

Shutts, G. J., 1986: A case study of eddy forcing during an Atlantic blocking episode. *Adv. Geophys.,* **29,** 135–162.

Sirutis, J., and K. Miyakoda, 1990: Subgrid-scale physics in 1-month forecasts. Part I: Experiment with four parameterization packages. *Mon. Wea. Rev.,* **118,** 1043–1064.

Smagorinsky, J., S. Manabe and J. L. Holloway, 1965: Numerical results from a nine-level general circulation model of the atmosphere. *Mon. Wea. Rev.,* **93,** 727–768.

Tibaldi, S., and L. R. Ji, 1983: On the effect of model resolution on numerical simulation of blocking. *Tellus,* **35A,** 28–38.

——, and F. Molteni, 1989: On the operational predictability of blocking. *ECMWF Workshop on The Nature and Prediction of Extra-Tropical Weather Systems,* Volume II, Reading, Berkshire, England, 329–371.

Tiedtke, M., 1983: Winter and summer simulations with the ECMWF model. *ECMWF Workshop on Intercomparison of Large-Scale Models Used for Extended Range Forecasts,* 263–313.

Treidle, R. A., E. C. Birch and P. Sajecki, 1981: Blocking action in the Northern Hemisphere: a climatological study. *Atmos.-Ocean,* **19,** 1–23.